doi:10.1093/mnras/stab866

Downloaded from https://academic.oup.com/mnras/article/503/4/6098/6189716 by University of Arizona Library user on 02 January 2024

Origins and demographics of wandering black holes

Angelo Ricarte,¹,2★ Michael Tremmel ®,³ Priyamvada Natarajan ®,³,4 Charlotte Zimmer⁵ and Thomas Quinn⁶

Accepted 2021 March 22. Received 2021 March 22; in original form 2021 February 18

ABSTRACT

We characterize the population of wandering black holes, defined as those physically offset from their halo centres, in the ROMULUS cosmological simulations. Unlike most other currently available cosmological simulations, black holes are seeded based on local gas properties and are permitted to evolve dynamically without being fixed at halo centres. Tracking these black holes allows us to make robust predictions about the offset population. We find that the number of wandering black holes scales roughly linearly with the halo mass, such that we expect thousands of wandering black holes in galaxy cluster haloes. Locally, these wanderers account for around 10 per cent of the local black hole mass budget once seed masses are accounted for. Yet for higher redshifts ($z \gtrsim 4$), wandering black holes both outweigh and outshine their central supermassive counterparts. Most wandering black holes, we find, remain close to the seed mass and originate from the centres of previously disrupted satellite galaxies. While most do not retain a resolved stellar counterpart, those that do are situated farther out at larger fractions of the virial radius. Wanderers with higher luminosities are preferentially at lower radius, more massive, and either closer to their host's mid-planes or associated with a stellar overdensity. This analysis shows that our current census of supermassive black holes is incomplete and that a substantial population of off-centre wanderers likely exists.

Key words: black hole physics – methods: numerical – galaxies: active.

1 INTRODUCTION

Every massive galaxy is believed to host a supermassive black hole (SMBH) at its centre (Kormendy & Richstone 1995; Kormendy & Ho 2013). SMBH masses correlate with properties of the inner regions of their host galaxies (Gebhardt et al. 2000; Ferrarese & Merritt 2000; Tremaine et al. 2002) that can be understood as the result of SMBH-galaxy co-evolution over cosmic time (e.g. Haehnelt, Natarajan & Rees 1998; Kauffmann & Haehnelt 2000; Volonteri, Haardt & Madau 2003; Somerville et al. 2008; Natarajan 2014). In the contemporary galaxy formation paradigm, SMBHs grow primarily from gas that makes its way to the galactic centre, resulting in active galactic nuclei (AGNs). Subsequently, feedback from the growing AGN helps quench star formation via radiation, winds, and/or jets (Di Matteo, Springel & Hernquist 2005; Springel, Di Matteo & Hernquist 2005; Croton et al. 2006; Sijacki et al. 2007). Modern cosmological simulations now self-consistently evolve star formation and SMBH growth from the early universe to the present day using sub-grid models for unresolved astrophysical processes, such as SMBH fuelling and feedback (Schaye et al. 2015; Bocquet et al. 2016; Dubois et al. 2016; Tremmel et al. 2017; Pillepich et al. 2018; Davé et al. 2019).

Hierarchical structure formation, whereby larger haloes result from the mergers of smaller ones, naturally produces SMBHs that are offset from the centres of their galaxies. The journey from galactic scales to the eventual SMBH merger in the inner regions of galaxies requires several different processes across a large dynamic range of spatial scales (Begelman, Blandford & Rees 1980; Colpi 2014). Only those secondary SMBHs that complete their journeys to the centres of their galaxies will form binaries with the primary SMBH, that can continue to evolve into the merger regime. It is possible that in some cases the orbital decay of these SMBHs can become stalled on scales much too large to form a bound binary (Governato, Colpi & Maraschi 1994; Schneider et al. 2002; Volonteri & Perna 2005; Callegari et al. 2009, 2011; Bellovary et al. 2010, 2021; Micic, Holley-Bockelmann & Sigurdsson 2011; Di Cintio et al. 2017; Dosopoulou & Antonini 2017; Dvorkin & Barausse 2017; Tamfal et al. 2018; Tremmel et al. 2018b).

First, on kilo-parsec scales, dynamical friction is the primary mechanism for angular momentum loss (Chandrasekhar 1943). For low enough SMBH masses, the dynamical friction time-scale can exceed the Hubble time. In addition, there has been a growing awareness that additional delays of Gyrs or longer can occur at this step, especially in clumpy high-redshift galaxies as noted in simulations (Biernacki, Teyssier & Bleuler 2017; Tremmel et al. 2018a; Pfister et al. 2019; Bortolas et al. 2020; Ma et al. 2021). Accreting SMBHs wandering on kilo-parsec scales can potentially

¹Center for Astrophysics | Harvard & Smithsonian, 60 Garden Street, Cambridge, MA 02138, USA

²Black Hole Initiative at Harvard University, 20 Garden Street, Cambridge, MA 02138, USA

³Department of Astronomy, Yale University, 52 Hillhouse Avenue, New Haven, CT 06511, USA

⁴Department of Physics, Yale University, P.O. Box 208121, New Haven, CT 06520, USA

⁵Department of Economics, Yale University, P.O. Box 208268, New Haven, CT 06520, USA

⁶Department of Astronomy, University of Washington, PO Box 351580, Seattle, WA 98195, USA

^{*} E-mail: angelo.ricarte@cfa.harvard.edu

be observed as dual/offset AGN (e.g. Comerford et al. 2009, 2013; Mezcua & Domínguez Sánchez 2020; Reines et al. 2020) or offset hyperluminous X-ray sources (King & Dehnen 2005; Barrows, Mezcua & Comerford 2019). There is also a growing sample of SMBH candidates observed in galactic haloes within ultra-compact dwarfs that may represent the stripped remnants of once-massive galaxies (Seth et al. 2014; Ahn et al. 2017; Afanasiev et al. 2018; Voggel et al. 2019).

In spherical symmetry, dynamical friction from stars becomes less efficient on parsec scales resulting in what has often been referred to as the 'final parsec problem' (Milosavljević & Merritt 2001, 2003). However, a wide variety of mechanisms has been proposed to overcome this barrier, including gas dynamical friction (Ostriker 1999; Escala et al. 2004; Armitage & Natarajan 2005; Mayer et al. 2007), individual gas clumps (Fiacconi et al. 2013; Goicovic et al. 2017), spherical asymmetry (Khan et al. 2013; Rantala et al. 2017; Gualandris et al. 2017), and even multibody interactions with other SMBHs (Ryu et al. 2018).

These journeys culminate in gravitational wave emission that can be detected by pulsar timing arrays and the planned Laser Interferometer Space Antenna (LISA) mission (Hobbs et al. 2010; Amaro-Seoane et al. 2017; Arzoumanian et al. 2020). Delays between halo merger and SMBH merger as discussed above can significantly impact gravitational wave event rates (Barausse et al. 2020). While there are several other sources of uncertainties in the current determination of LISA merger event rates from SMBH mergers, including those arising from accretion physics, and the hitherto unknown formation mechanisms for initial black hole seeds (Sesana, Volonteri & Haardt 2007; Klein et al. 2016; Ricarte & Natarajan 2018b; Dayal et al. 2019), the role of SMBH dynamics prior to reaching the gravitational wave regime is one of the key unknowns. The SMBH merger rate can also have a significant impact on SMBH mass and spin evolution, especially in the most massive galaxies (Volonteri et al. 2005, 2013). Several models predict that SMBH mergers can contribute significantly to the mass budgets of the most massive low-redshift SMBHs, those hosted by gas-poor ellipticals (Kulier et al. 2015; Ricarte & Natarajan 2018a; Pacucci & Loeb 2020).

Cosmological simulations can be powerful tools for predicting the formation of SMBH binaries because they naturally include realistic merger histories and self-consistently evolving galaxies and largescale structure. The ROMULUS cosmological simulations (Tremmel et al. 2017) are one of the only large-scale simulations that selfconsistently tracks the orbital evolution of SMBH pairs down to sub-kpc scales through the use of a sub-grid dynamical friction prescription to account for missing dynamical friction from stars and dark matter (but not gas; Tremmel et al. 2015). ROMULUS is therefore uniquely able to predict which SMBHs, following a galaxy merger, will actually make it to the centre of their new host galaxy and how long that process will take. Indeed, as presented in Tremmel et al. (2018a), ROMULUS predicts that many SMBH binaries form after several Gyrs of orbital evolution, while some SMBHs will never make it to the centre. As a result, Milky Way-mass galaxies in ROMULUS are found to host an average of 12 SMBHs that typically wander the halo far from galactic centre (Tremmel et al. 2018b).

In this work, we perform a detailed study of the ROMULUS suite of simulations to characterize the population of wandering SMBHs beyond the centres of their host haloes. The outline of paper is as follows: in Section 2, we provide a brief summary of the ROMULUS simulations, focusing on the SMBH physics and the post-processing necessary to perform this study. In Section 3, we present the results of this analysis and present the detailed properties of this population:

bulk properties in Section 3.1, intra-halo statistics in Section 3.2, and a study of stellar counterparts in Section 3.3. We discuss the caveats and broader implications of this study in Section 4, and summarize our results in Section 5.

2 METHODOLOGY

In this work, we present results from analysis of the ROMULUS suite of simulations, both ROMULUS25 and ROMULUSC.

2.1 The ROMULUS Simulations

Here, we summarize the important aspects of the SMBH physics implemented in the ROMULUS simulations that is relevant to our current discussion, further details can be found in Tremmel et al. (2017, 2019). The ROMULUS simulations consist of ROMULUS25, a (25 mpc)³ volume, and ROMULUSC, a zoom-in on a $10^{14}\,M_{\odot}$ galaxy cluster. These simulations utilize the Tree + Smoothed Particle Hydrodynamics (SPH) code CHANGA (Menon et al. 2015; Wadsley, Keller & Quinn 2017), with a dark matter particle mass of $3.39\times10^5\,M_{\odot}$ and a gas particle mass of $2.12\times10^5\,M_{\odot}$.

SMBHs in both simulations are seeded based on local gas properties, without any knowledge of the host halo or galaxy. As a consequence, not all haloes are explicitly guaranteed to host a SMBH, and multiple SMBHs may form in the same halo. A gas particle that would have formed a star instead is transformed into a SMBH if all of the following hold true:

- (i) It is very metal poor, with metallicity $Z < 3 \times 10^{-4}$.
- (ii) It is very dense, at least 15 times the star forming threshold of $0.2 m_n \text{ cc}^{-1}$.
 - (iii) It is warm, with a temperature between 9500 and 10000 K.

This seeding prescription emulates the direct collapse black hole scenario, where the high temperatures and low metallicities allow for a large Jeans mass that can directly collapse into a SMBH seed (Oh & Haiman 2002; Bromm & Loeb 2003; Begelman, Volonteri & Rees 2006; Lodato & Natarajan 2006). SMBHs are seeded with an initial mass of 10^6 M_{\odot} to ensure that they are always more massive than other particles in the simulation that could otherwise cause spurious scattering events. Due to this local seeding prescription, SMBHs will occasionally form very close to each other and promptly merge, but this does not occur for the majority of SMBHs. As discussed in Tremmel et al. (2018a), the majority of wandering SMBHs in Milky Way mass haloes have not experienced any mergers, nor have grown beyond twice their seed mass. The vast majority (>90 per cent) of SMBHs are seeded at redshifts $z \ge 5$, well prior to epochs studied in this work. At the lower redshifts studied here, the inferred properties of the wandering population are no longer dominated by the initial conditions pertinent to their formation.

Gravity in the Romulus suite is softened below 350 pc using a spline kernel, equivalent to 250 pc Plummer softening length. The dynamical friction force on to SMBHs is corrected for the underestimate due to this softening, and this is done by integrating the Chandrasekhar (1943) dynamical friction equation within the smoothing radius (Tremmel et al. 2015). With the addition of this force correction, SMBHs are allowed to orbit freely without being explicitly pinned to the centres of their haloes. Note that the ROMULUS simulations do not account for dynamical friction from gas (Ostriker 1999). Such gas drag has been included in other large-scale simulations, but without the effects of stars and dark matter (Dubois et al. 2014). The effect of gas may become particluarly important at

high redshift (though see recent results from Pfister et al. 2019 for further discussion).

Two SMBHs merge if they are within two gravitational softening lengths (within 0.7 kpc) and have low enough relative velocities to be considered bound. That is, if $\frac{1}{2}\Delta\vec{v} < \Delta\vec{a} \cdot \Delta\vec{r}$, where $\Delta\vec{v}$ is the relative velocity, $\Delta\vec{a}$ is the relative acceleration, and $\Delta\vec{r}$ is the relative displacement of two SMBHs (Bellovary et al. 2011).

Further, in these simulations, SMBHs accrete based on the Bondi– Hoyle–Lyttleton formula (Bondi 1952), modified to account for angular momentum support. The accretion rate is given by

$$\dot{M}_{\bullet} = \alpha(n) \begin{cases} \frac{\pi (GM_{\bullet})^2 \rho}{\left(v_{\text{bulk}}^2 + c_s^2\right)^{3/2}} & \text{if } v_{\text{bulk}} > v_{\theta} \\ \frac{\pi (GM_{\bullet})^2 \rho c_s}{\left(v_{\theta}^2 + c_s^2\right)^2} & \text{if } v_{\text{bulk}} < v_{\theta}, \end{cases}$$
(1)

where G is the gravitational constant, M_{\bullet} is the SMBH mass, ρ is the ambient mass density, c_s is the ambient sound speed, v_{θ} is the local rotational velocity of surrounding gas, and v_{bulk} is the bulk velocity relative to the SMBH (see Tremmel et al. 2017 for additional details). Ambient quantities are calculated using the 32 closest gas particles. The coefficient $\alpha(n)$ is a number density-dependent boost factor given by

$$\alpha(n) = \begin{cases} \left(\frac{n}{n_{\text{th},*}}\right)^2 & \text{if } n \ge n_{\text{th},*} \\ 1 & \text{if } n < n_{\text{th},*} \end{cases}, \tag{2}$$

where $n_{\text{th, *}}$ is the star formation number density threshold, meant to represent the limit beyond which the simulation no longer resolves the multiphase interstellar medium (Booth & Schaye 2009).

To model AGN feedback, thermal energy is isotropically imparted into nearby gas particles during accretion, assuming a radiative efficiency of 10 per cent, and a feedback coupling efficiency of 2 per cent. There is no separate kinetic/radio mode included in the AGN feedback implementation. Details of the sub-grid physical processes that describe star formation and feedback from the stellar population as well as the growing SMBH are described in Tremmel et al. (2017, 2019).

2.2 Post-processing: finding the wandering population

We use the AMIGA halo finder to define haloes and derive their virial masses, virial radii, and centres (Knollmann & Knebe 2009). We require each halo to have at least 104 dark matter particles for it to be considered well resolved. Outputs are processed using The Agile Numerical Galaxy Organisation System (TANGOS; Pontzen & Tremmel 2018). AMIGA assigns SMBHs to a halo, along with all other dark matter, star, and gas particles, based on whether or not the objects are bound to the structure. SMBHs may also be assigned to substructure within more massive haloes. Halo centres are determined using the shrinking-spheres approach (Power et al. 2003) that consistently traces the centres of central galaxies as well. This method determines halo centres with a precision approximately equal to the gravitational softening length, within which gravity is not resolved and the potential minimum cannot be accurately defined. For ROMULUS this is 350 pc. The calculation may be further complicated and uncertain during on-going halo/galaxy mergers of similar mass, although we do not expect this to systematically affect our results.

We define a SMBH to be 'central' if it is within 0.7 kpc of the halo centre (twice the gravitational softening length), and 'wandering' if it lies anywhere beyond this radius. This definition allows for multiple central SMBHs in the same halo, and also permits the most central, massive, or luminous SMBH in a halo to be designated as wandering.

The minimum threshold of 0.7 kpc takes into account uncertainties in the SMBH dynamics, as well as the definition of the centre of the galaxy, due to the gravitational softening length. This is also the distance threshold within which two SMBHs are allowed to merge (due to the unreliable dynamics at these scales). Outside of 0.7 kpc we can be confident that gravity and the dynamical evolution is fully resolved and the SMBH particles are not about to merge within the simulation. To further study the wandering population, we consider three different radial cuts for their locations ranging from the most generous to a more stringent definition as follows:

- (i) All SMBHs beyond 0.7 kpc, such that the wandering SMBH population is the complement of the central SMBH population.
 - (ii) All SMBHs beyond 5 kpc, a more conservative cut.
 - (iii) All SMBHs beyond 0.1 R_{200} , as calculated for each halo.

The first cut is the most inclusive classification criteria, the second extends out to a physical scale that corresponds roughly the size scale of the visible galaxy, and the final cut is the tightest aligned with the most stringent definition for a wanderer.

When we present data binned by halo mass, we combine haloes from the ROMULUS25 (the field) and ROMULUSC (the cluster) simulations by only using ROMULUSC data to extend into halo mass bins for which ROMULUS25 has no data. We refrain from including ROMULUSC galaxies in less massive bins because environmental effects (such as tidal stripping and ram pressure stripping) significantly modify lower mass galaxies in the cluster environment compared to their counterparts in the field. At z=0.05, the lowest redshift for which we analyse these simulations, the most massive halo in ROMULUS25 is a galaxy group with a mass of $2.1\times10^{13}~{\rm M}_{\odot}$, while the main halo of cluster simulation ROMULUSC has a mass of $1.4\times10^{14}~{\rm M}_{\odot}$.

3 RESULTS

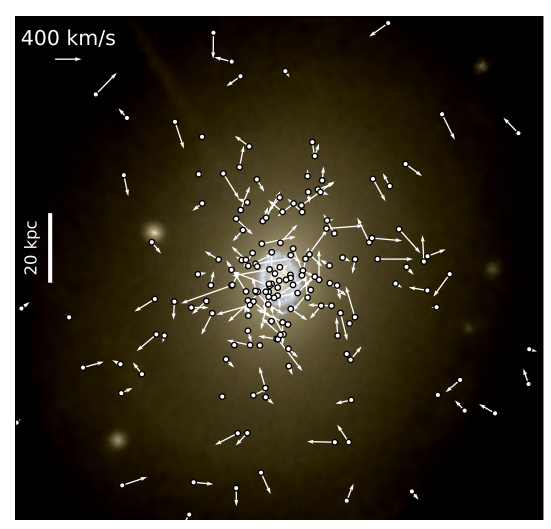
In Section 3.1, we study bulk statistics of wandering SMBHs compared to their central counterparts, including their total masses and luminosities. Then, in Section 3.2, we then study the intra-halo statistics of the population, such as their mass function and radial distribution. Lastly, in Section 3.3, we examine whether or not wandering SMBHs may reveal their presence via a stellar overdensity.

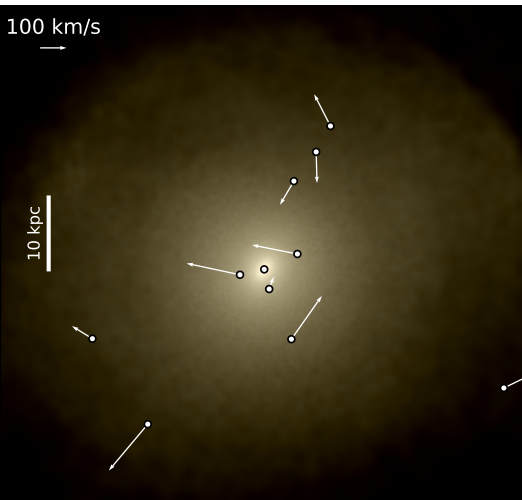
3.1 Population statistics

3.1.1 Central and wanderer abundances

Wandering SMBHs are ubiquitous in the ROMULUS simulations, and occur in greater numbers in more massive haloes. In Fig. 1, we plot three sample images of galaxies selected to span two decades in halo mass. From top to bottom, these galaxies reside in haloes with virial masses of $2\times 10^{13}\,M_\odot,^1~2\times 10^{12}~M_\odot$, and $2\times 10^{11}~M_\odot$, respectively. The location and velocity of each SMBH bound to the halo is marked with a circle and an associated arrow. These haloes host 241, 15, and 2 wanderers, respectively (not all of which fit in the images shown), consistent with a linear trend with halo mass. As we further explore in Section 3.2.2, wandering SMBHs span a broad range of distances, extending all the way out to the virial radius. These images are generated assuming a surface brightness limit of 28 mag arcsec $^{-2}$ to better visualise the stellar halo. Even at this faint surface brightness limit, the wandering SMBHs are not associated with stellar counterparts.

¹The blue stars visible in this halo reflect a recent merger event.





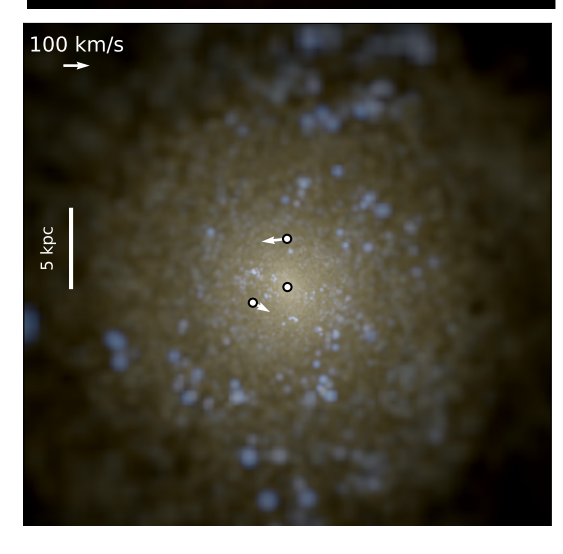


Figure 1. Examples of wandering SMBH populations of galaxies in ROMULUS25, stepping through two decades in halo mass. From top to bottom, these haloes have virial masses of $2 \times 10^{13} \, \mathrm{M_\odot}$, $2 \times 10^{12} \, \mathrm{M_\odot}$, and $2 \times 10^{11} \, \mathrm{M_\odot}$, respectively. The total number of wanderers in each galaxy is 241, 15, and 2, respectively, following a linear scaling between number of wanderers and halo mass. Images are generated assuming a faint surface brightness limit of 28 mag arcsec⁻². Note the different size and velocity scales in each panel.

In Fig. 2, we plot as a function of halo mass the average number of central SMBHs in the top row, and the average number of wandering SMBHs (using the three different definitions outlined in Section 2.2) in the bottom row for three different redshifts. We write the number of haloes that exist in each bin above of the error bars in the top row. Miller et al. (2015) estimate the SMBH occupation fraction at z=0 as a function of stellar mass, and we overplot their observational results in green after applying the stellar-to-halo mass relation of Moster et al. (2013). In this figure, and subsequent figures in this section, error bars in the vertical direction enclose the 16th to 84th percentile regions regions (meant to represent 1σ), estimated via bootstrapping the haloes in a given mass bin.

There is a remarkable level of agreement between the average number of centrals in ROMULUS and the locally observed occupation fraction. Recall that the SMBH seeding prescription used in ROMULUS is based on local gas properties, without any knowledge of global halo properties. Almost all seeds are established by $z \gtrsim$ 5, and the occupation fraction at z = 0 depends on a combination of seeding, growth, and dynamical processes that bring SMBHs into galaxy centres. It is thus notable that observations and predictions from ROMULUS agree at this level despite the modelling uncertainties in all three of the these processes, which bolsters our confidence that ROMULUS produces a reasonable population of wandering SMBHs. The distributions at z = 1 and z = 3 follow the same general shape as the local bin, though interestingly, the average number of central SMBHs exceeds unity in the highest mass bins at z = 3. Recall that SMBHs merge in ROMULUS not only if they are within two gravitational smoothing lengths, but also if they have small enough relative velocities to be considered bound. We were surprised to find a few massive galaxies at z = 3 in ROMULUS that host multiple central SMBHs that obviously meet the spatial separation criterion but not the velocity criterion for merging, resulting in multiple centrals.

In the bottom row, we find that the number of wandering SMBHs exceeds unity for $M_{200} \gtrsim 10^{11} \ {\rm M_{\odot}}$ at all three epochs and that for larger halo masses the abundance of wanderers is significantly larger. The number of wandering SMBHs scales roughly linearly with the halo mass, a trend stretching from dwarf galaxy haloes to galaxy clusters. We find additional structure if stellar mass bins are adopted instead, due to the non-linear mapping between stellar and halo mass, suggesting that halo mass is the more fundamental property. A power-law regression (linear in logarithmic space) to the number of wanderers as a function of halo mass is plotted as the dashed line. This linearity holds regardless of the distance cut from the galaxy centre chosen to define wanderers, although a steeper slope is obtained using the 5 kpc cut. This is unsurprising as 5 kpc is an evolving fraction of the virial radius depending on the host halo mass and redshift. At z = 0.05, for the >0.7 kpc, >5 kpc, and >0.1 R_{200} populations, we find: $\log_{10} N_w = 1.15 [\log_{10} (M_{200}/10^{12} \,\mathrm{M}_{\odot})] + 0.93$, $\log_{10}N_w = 1.31[\log_{10}(M_{200}/10^{12} \,\mathrm{M}_{\odot})] + 0.72$, and $\log_{10}N_w =$ $1.26[\log_{10}(M_{200}/10^{12} \,\mathrm{M}_{\odot})] + 0.42$, respectively. In low mass haloes, the number of wanderers increases with increasing redshift, reflecting the redshift evolution of the SMBH occupation fraction.

In earlier work with these simulations, Tremmel et al. (2018b) determined that Milky Way mass haloes host 12.2 ± 8.4 SMBHs within their virial radii, consistent with these results. Meanwhile, the main cluster mass halo of the cluster simulation ROMULUSC, with a virial mass of 10^{14} M $_{\odot}$ at z=0.05, hosts a staggering 1613 wandering SMBHs, excluding those that are associated with individual galaxy scale subhalos. We cautiously note here that halo finders have difficulty identifying substructure in dense galaxy clusters, such that some of these wandering SMBHs could potentially reside in undetected subhalos. In an investigation of mass segregation, Joshi,

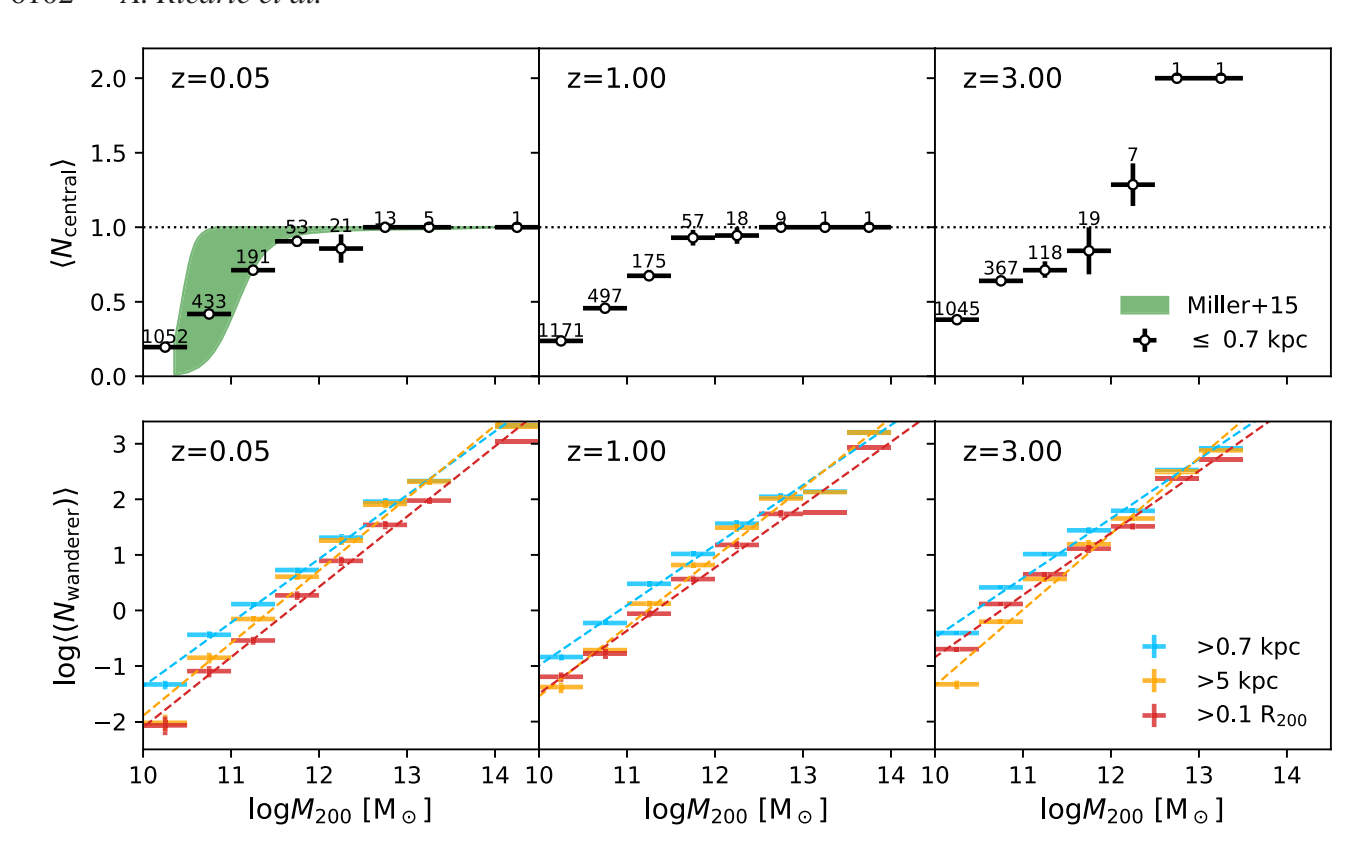


Figure 2. Average numbers of central SMBHs (above) and wandering SMBHs (below) as a function of halo mass for three different redshifts in ROMULUS. Different colours reflect different cuts of the wandering population, while the numbers above the error bars in the top row are the number of unique haloes in each bin. We compare the number of central SMBHs at the lowest redshift with the occupation fraction estimate of Miller et al. (2015), after applying the stellar-to-halo mass relation of Moster, Naab & White (2013) and find remarkable agreement despite the seeding mechanism lacking any knowledge of global halo properties. Interestingly, we find that the most massive haloes at z = 3 sometimes host an extra central SMBH, requiring that they have too large relative velocities to be considered bound. A power law fit to the number of wandering SMBHs as a function of halo mass is plotted using dashed lines. The number of wanderers scales roughly linearly with the halo mass at all redshifts. At all epochs, wandering SMBHs far outnumber central SMBHs in all except dwarf galaxy haloes.

Parker & Wadsley (2016) compared the ROCKSTAR and AMIGA halo finders and determined that the mass attributed to sub-haloes was inconsistent between the two halo finders inside approximately 0.2 times the virial radius. In the main halo of ROMULUSC, 70 per cent of wandering SMBHs are within $0.2R_{200}$ at z=0.05. Nevertheless, the number of wanderers in the cluster halo is consistent with extrapolating the linear trend found at lower masses (as shown in the lower panel of Fig. 2).

3.1.2 Central and wanderer masses

To hone in on the growth history of these wanderers, we study the amount of mass locked up in wandering SMBHs as well as their accretion rates. These estimates have important implications for the Soltan (1982) argument that connects the evolving AGN luminosity function (actively accreting SMBHs) to the total mass accumulated in relic central SMBHs as measured at z=0. AGN emission is frequently used to estimate the cosmic SMBH growth rate at a given epoch, which when integrated from high redshift to the present day is set to equal to the mass of central SMBHs at z=0 (e.g. Haehnelt et al. 1998; Hopkins, Richards & Hernquist 2007; Merloni & Heinz 2008; Ananna et al. 2020; Shen et al. 2020). Mass locked in wandering SMBHs is not accounted for in the Soltan argument and therefore represents a missing term from the right-hand side of the equation.

In Fig. 3, we first plot the average total mass included in *all* central or wandering SMBHs as a function of halo mass in ROMULUS25. Only

the accreted portion of a SMBH's mass is included, removing the masses from all seeds that have merged to form the final product, which is the direct comparison for the Soltan argument. As shown in Ricarte et al. (2019), the accreted mass is strongly correlated with the host stellar mass even when the accreted mass falls below the initial seed mass of $10^6~M_{\odot}$. Since most wandering SMBHs do not grow substantially from their initial seed mass, this also allows us to better differentiate the population of wanderers in terms of mass and allows us to make conservative estimates of the amount of mass locked up in wanderers.

As with their total numbers, both central and wandering SMBH masses follow linear trends with halo mass. At z = 0, note that the sub-grid parameters of these simulations are tuned to reproduce the empirically measured central SMBH mass to stellar mass relation (specifically Schramm & Silverman 2013), and hence a linear relationship between $M_{\bullet, acc}$ and M_{200} for central SMBHs exists by construction. Nevertheless, it is interesting that the linear relationship extends down to haloes of even $10^{10} \,\mathrm{M}_{\odot}$, far below the mass threshold above which AGN feedback is thought to quench galaxies and shape their properties. Overall, we find that wandering SMBHs produce only a roughly 10 per cent correction to the total amount of accreted mass locked up in SMBHs at z = 0, which is small compared to the systematic uncertainties on scaling relations used to estimate the total mass locked up in SMBHs (Kormendy & Ho 2013; Reines & Volonteri 2015; Saglia et al. 2016; Shankar et al. 2016).

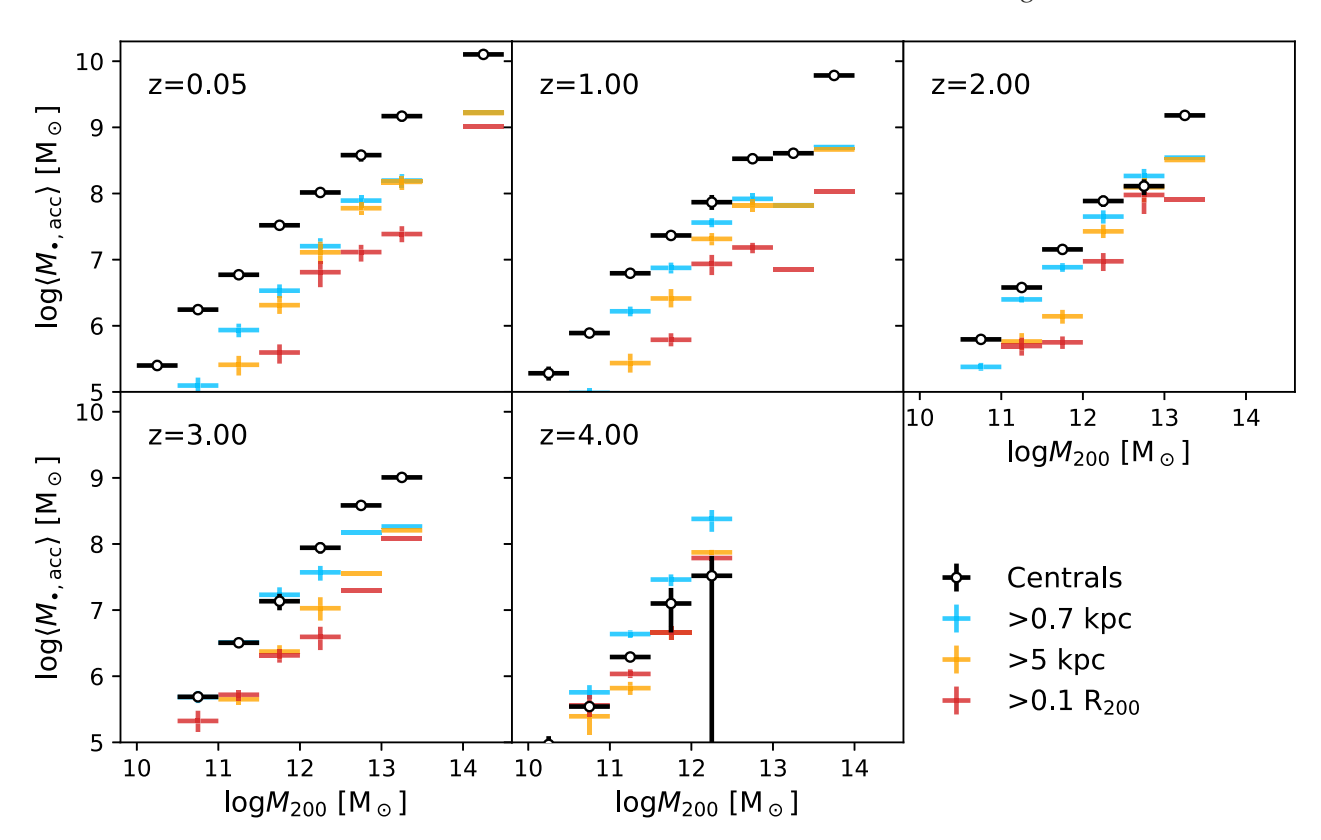


Figure 3. Average amount of mass in central and wandering SMBHs as a function of halo mass and redshift. Only the accreted portion of SMBH masses are included, which excludes all seed masses. The fraction of mass in wandering SMBHs is roughly 10 per cent the mass in central SMBHs at z = 0.05, but this fraction increases with redshift. At z = 4, the mass locked in wanderers exceeds that locked in centrals, likely due to the increased merger rate at high redshift.

However, we find that as redshift increases, the fraction of mass tied up in SMBH wanderers increases, such that wandering SMBHs actually dominate the black hole mass budget at z=4. This is despite the fact that dynamical times are shorter at high redshift (e.g. Barkana & Loeb 2001). This suggests that the increased merger rate at high redshift is reflected in and results in the existence of wandering SMBHs. Higher redshift galaxies simulated in a cosmological environment are also clumpier, which can disrupt the angular momentum loss of wanderers via scattering events (Pfister et al. 2019; Bortolas et al. 2020; Ma et al. 2021).

3.1.3 Central and wanderer luminosities

We now examine if this wandering population implies and results in a corresponding increase in detectable emission. A variety of models predict that wandering SMBHs can manifest as off-nuclear X-ray or radio sources (Fujita 2008, 2009; Bellovary et al. 2010; Sijacki, Springel & Haehnelt 2011; Kawaguchi et al. 2014; Steinborn et al. 2016; Barrows et al. 2019; Zivancev, Ostriker & Küpper 2020; Guo et al. 2020; Bartlett et al. 2021). In Fig. 4, we plot the average total bolometric luminosities of *all* central or wandering SMBHs as a function of halo mass in ROMULUS25. In order to mitigate AGN variability, luminosities are averaged over 30 Myr. Self-consistently with the feedback prescription used in ROMULUS, we assume a universal radiative efficiency of 10 per cent for all sources; $L_{\rm bol} = 0.1 \dot{M}_{\bullet} c^2$, where \dot{M}_{\bullet} is the SMBH growth rate and c is the speed of light.

Similar to the mass budget, we find that wandering SMBHs beyond 0.7 kpc can indeed contribute a significant amount to the total AGN

photon budget of a halo, growing with redshift. As suggested by their mass budgets, wandering SMBHs cumulatively outshine central SMBHs at z=4.0. However, we also notice an interesting change in behaviour in the most massive haloes at low redshift. Although both the total number and total mass of wandering SMBHs continues to increase with halo mass, their cumulative accretion rates begin to decline in the group and cluster haloes. This is likely a consequence of AGN feedback from the central SMBH heating the gas in the most massive haloes. Unfortunately, this means that despite their high abundance, wandering SMBHs will be more difficult to detect via emission in group and cluster environments.

3.2 Intra-halo statistics

3.2.1 The (accreted) mass function of wandering SMBHs

Here, we explore the mass functions of wandering SMBHs in Fig. 5. Banik et al. (2019) found a Schechter-like wandering SMBH mass function in ROMULUS25, and here we search for trends in halo mass and redshift. We again plot only the accreted portion of a SMBH's mass, excluding the initial seed mass. The *y*-axis represents the fraction of SMBHs with accreted masses above that listed on the *x*-axis. Different colours represent different halo masses, and the dashed vertical lines plot the median central SMBH mass in a given halo mass bin. We find that the mass function of wandering SMBHs is dominated by SMBHs with accreted masses less than the seed mass of $10^6\,\mathrm{M}_\odot$. That is, most of these wandering SMBHs never grew by a substantial fraction of their initial masses in the simulation. Less than approximately 10 per cent of them have accreted masses greater than the seed mass.

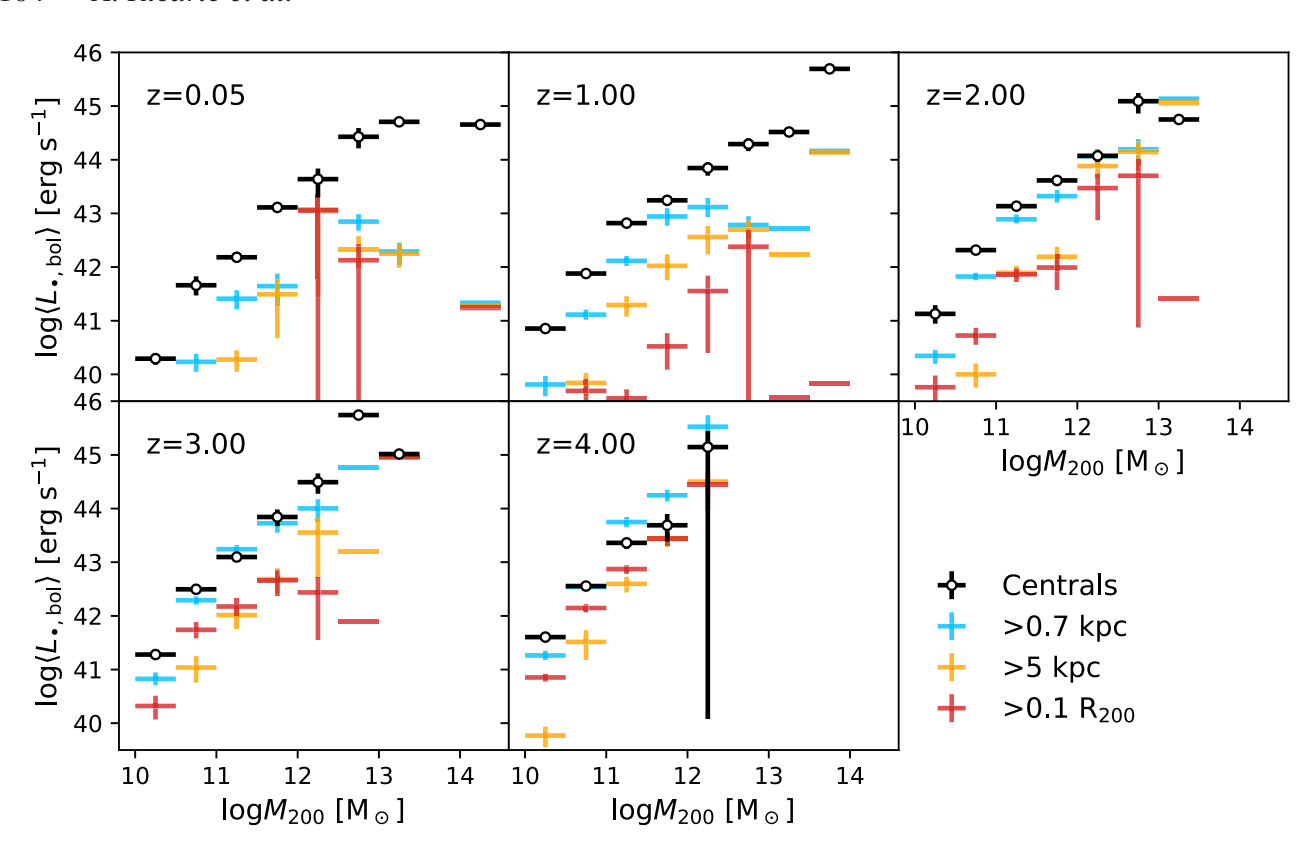


Figure 4. Average luminosities of central and wandering SMBH populations as a function of halo mass. Wandering SMBHs outshine centrals in massive haloes at z = 4. Wandering luminosities are suppressed in massive haloes at low redshift, most likely due to AGN feedback from the central SMBH.

The universality of these curves is remarkable. Despite the median central mass increasing dramatically with halo mass, the mass function of wandering SMBHs remains nearly the same. This behaviour can be anticipated based on Figs 2 and 3: both the number of wanderers and their cumulative masses are roughly linear with halo mass, implying that the typical wanderer mass does not change. We do note, however, that more massive haloes exhibit a larger tail of massive wanderers. This is because, as we will further explore, wandering SMBHs originate from minor mergers.

3.2.2 Spatial distributions

In Fig. 6, we plot radial distributions of wandering SMBHs as a function of virial radius for three different redshifts. The peaks of these distributions tend to occur at roughly at a tenth of the virial radius, moving outward with increasing halo mass. There is a wide tail to large offsets that also increases with halo mass. The spatial distribution of wandering SMBHs spans the full radial extent of the halo, although they remain much more centrally concentrated than the dark matter halo itself. In the main ROMULUSC halo at z=0.05 (the sole halo in the $10^{14-14.5}~{\rm M}_{\odot}$ bin), a substantial population of wanderers can be found all the way out to the virial radius. This distribution is robust and does not appear to change substantially with redshift.

Unsurprisingly, the emission generated by these wandering SMBHs is more biased towards smaller radius than the population overall. At smaller radius, the ambient gas is both denser and colder. This is shown in Fig. 7, where we plot the average luminosity profile of haloes of different mass for comparison with Fig. 6. Notice again

the depression of the luminosity in the most massive bin compared to much less massive haloes.

A deeper analysis reveals additional factors that promote growth on to wandering SMBHs. In Fig. 8 we plot $\sin(\theta_p)$ as a function of bolometric luminosity (averaged over 30 Myr) for each wandering SMBH at z = 0.05. Here, θ_p is the angle made between each SMBH's position vector (from the center of its host halo) and the disk. (By plotting $\sin(\theta_p)$ instead of θ_p , we ensure that the y-axis evenly samples solid angle.) If we detect a stellar overdensity of at least a factor 10 (see Section 3.3 for details), we mark these SMBHs with stars instead of circles. The error bars represent the 16th, 50th, and 84th percentile regions, revealing that the more luminous wandering SMBHs are more likely to be close to the disk plane, as expected from previous studies (Volonteri & Perna 2005; Fujita 2009). In addition, colours encode SMBH mass, revealing that the more luminous wanderers are also more likely to be more massive, as expected from the Bondi accretion formula. When passing through the galactic disk, wandering SMBHs may also produce an observable bow shock (Wang & Loeb 2014).

3.3 Do wanderers retain stellar counterparts?

We explore whether or not wandering SMBHs reside in stellar overdensities by examining the particle data at redshift z=0.05. If wandering SMBHs retain a stellar counterpart, this can make them easier to find. This also serves as a test of our halo finder, which may have difficulty identifying low-mass haloes in crowded environments.

We define the local stellar mass density, denoted $\rho_{*, local}$, to be equal to the mass density of stars within a sphere with a 1 kpc radius

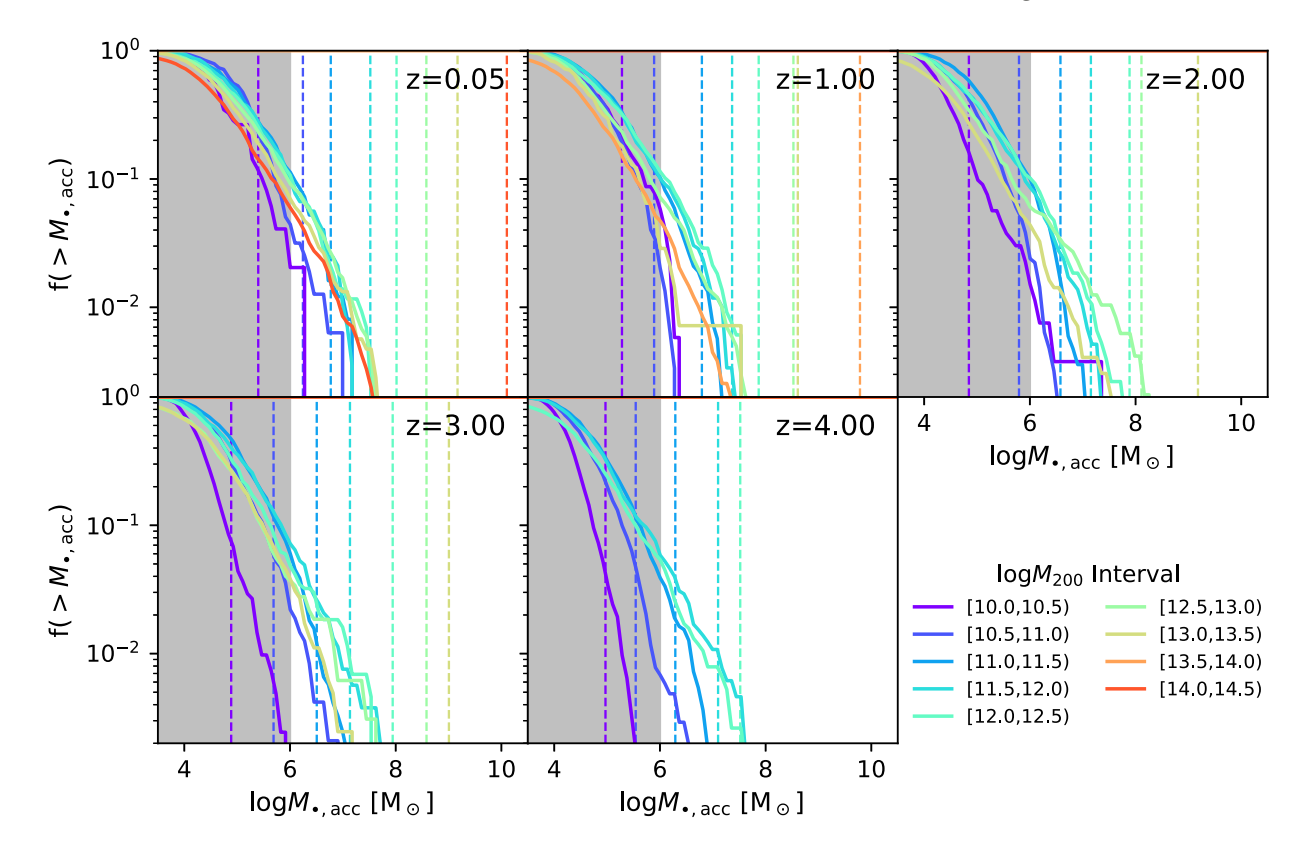


Figure 5. Mass function of wandering SMBHs as a function of halo mass and redshift. Only the accreted portions of mass are included, which excludes seed masses. Vertical dashed lines plot the median *central* SMBH mass at a given halo mass. Mass functions of wandering SMBHs are very similar as a function of halo mass and redshift, even though central SMBH masses are highly halo mass dependent. The vast majority of wandering SMBHs have accreted masses below the seed mass of $10^6 \, M_{\odot}$ (within the grey-coloured region).

centered on a given wandering SMBH. Then, for comparison, we compute the typical stellar mass density of the SMBH's host halo at comparable radius and disk height, $\rho_{*, halo}$. To be more explicit, we select star particles within the intersection of (i) a spherical shell that encloses but excludes the aforementioned 1 kpc radius sphere, and (ii) the region defined by $|z-z_{\bullet}| \leq 1$ kpc, where z_{\bullet} is the vertical distance that the wandering SMBH is away from the galactic mid-plane, located using PYNBODY's 'faceon' function (Pontzen et al. 2013). We exclude wandering SMBHs that reside in haloes for which this function fails to determine an angular momentum vector, which amounts to 20 per cent of the total number of wanderers.

Results are plotted in Fig. 9. The ratio $\rho_{*,\, local}/\rho_{*,\, halo}$ is plotted as a function of host halo mass, $M_{200,\, host}$. Colours encode the ratio of the SMBH's halo-centric distance to the host virial radius. Overall, the majority of wandering SMBHs appear to exist in ambient stellar densities typical for the halo overall, implying that the haloes in which they formed have been completely tidal disrupted. Some exceptions exist, however, and as revealed by the colouration, those SMBHs which do reside in stellar overdensities tend to exist a large halo-centric radius. These SMBHs likely retain a stellar component due to the weaker tidal forces in the halo outskirts. Fortunately, these cases are not likely to be due to halo finder inaccuracies, which would have greater difficulty identifying substructure at small radius rather than at large.

The fact that wandering SMBHs typically do not exist in stellar overdensities except at large radius bolsters our confidence that we are not simply selecting for SMBHs in regions where the halo finder has a difficult time identifying substructure. We note that the 350 pc resolution of this simulation disallows the formation of potentially

denser stellar structures like nuclear star clusters that are found in approximately 70 per cent of galaxies with less than $10^{11}\,\rm M_\odot$ in stars (Neumayer, Seth & Böker 2020). Nuclear star clusters may well be the birthplaces of SMBH seeds (Devecchi & Volonteri 2009; Alexander & Natarajan 2014; Natarajan 2021), and may also be an additional source of wanderers if they form offset from their galactic centres. Such dense stellar structures can more easily avoid tidal disruption and also help SMBHs to sink more efficiently to the centre of galaxies (Van Wassenhove et al. 2014; Tremmel et al. 2018a). Finally, numerical disruption is known to artificially destroy the innermost bound clumps of haloes experiencing tidal stripping, which may also cause ROMULUS to underestimate the local stellar and dark matter density around wandering SMBHs (van den Bosch & Ogiya 2018).

4 DISCUSSION

From our detailed study, we report that wandering SMBHs are plentiful in the ROMULUS universe, with numbers scaling linearly with the halo mass. Their masses imply only a roughly 10 per cent correction to the total mass locked up in SMBHs locally, but they may collectively outweigh the contribution from central SMBHs at high redshifts when galaxy mergers are more frequent. We find that wanderers typically have very low masses (similar to their initial seed masses) and do not typically reside in halo overdensities, with a large fraction lying beyond the visible extent of their hosts. Here, we discuss some of the numerical limitations and broader implications of this study.

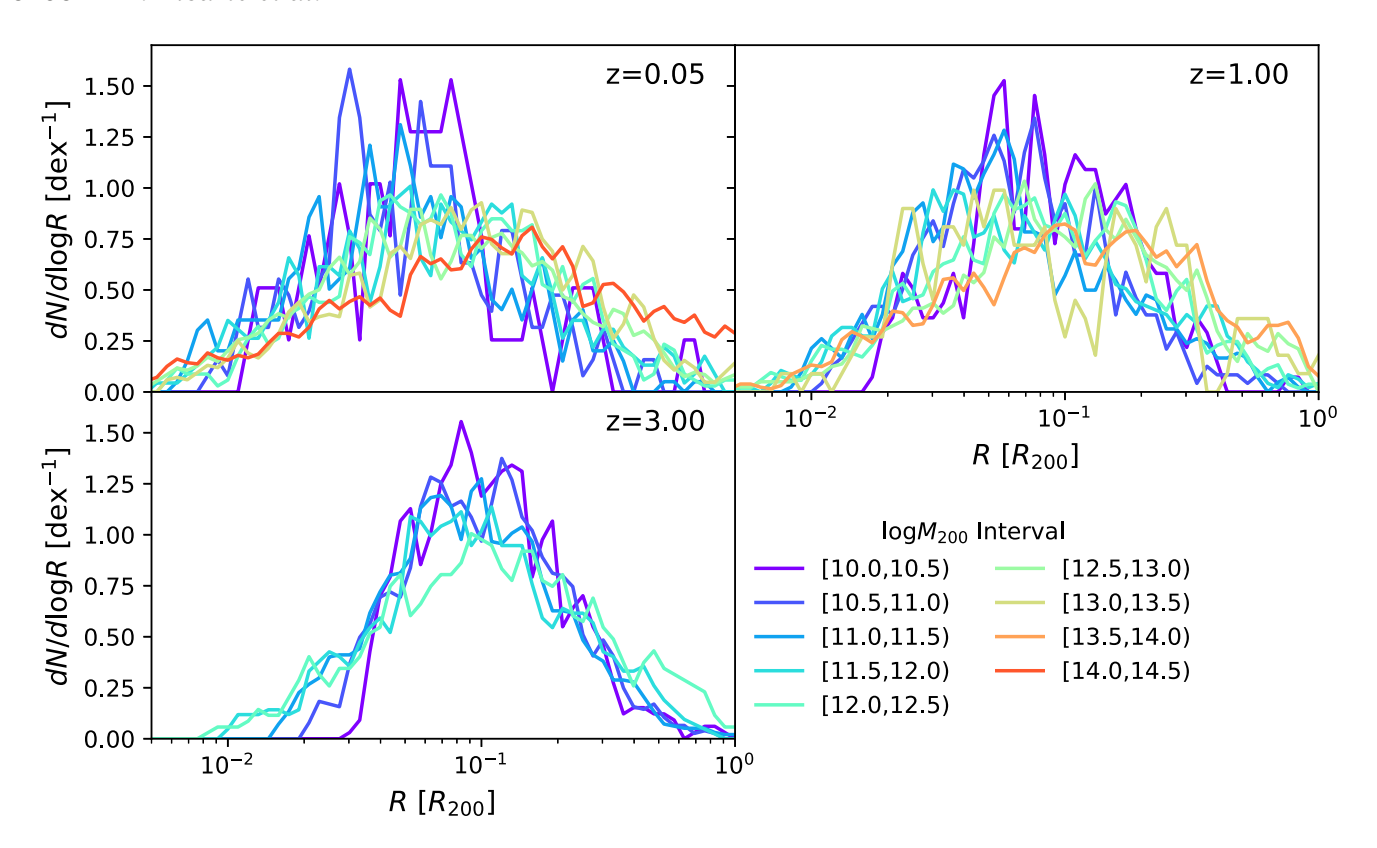


Figure 6. Spatial distributions of wandering SMBHs in the ROMULUS simulations as a function of virial radius. Different colours correspond to different bins in halo mass. We find a broad distribution of radii with a peak at roughly a tenth the virial radius that moves outward as halo mass increases. Different panels depict different redshifts, over which we do not see substantial evolution.

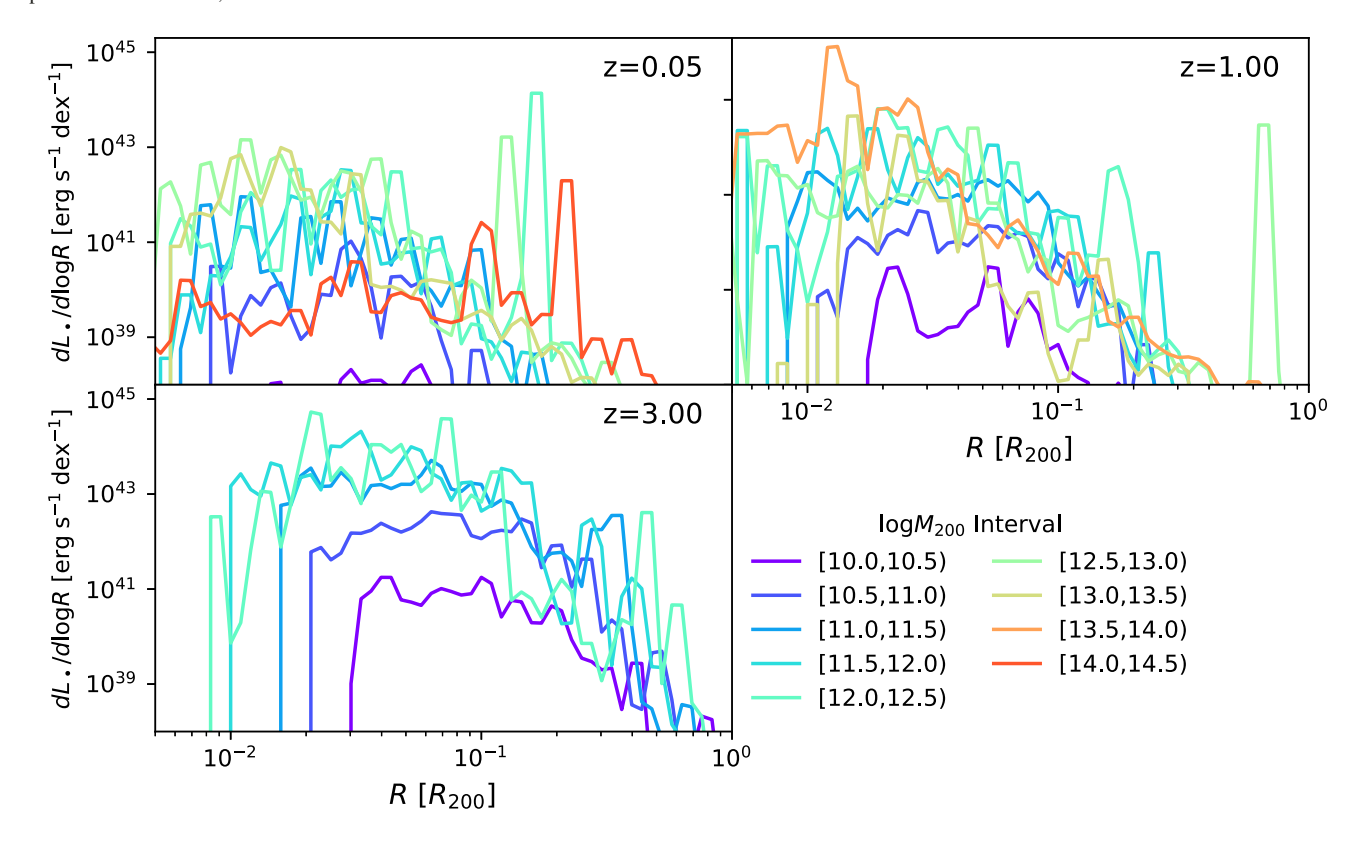


Figure 7. Bolometric luminosity distributions of wandering SMBHs as a function of virial radius for three different redshifts, assuming a radiative efficiency of 0.1. Comparing with Fig. 6, these distributions are more centrally concentrated than the population overall, since gas is both denser and colder at smaller radius.

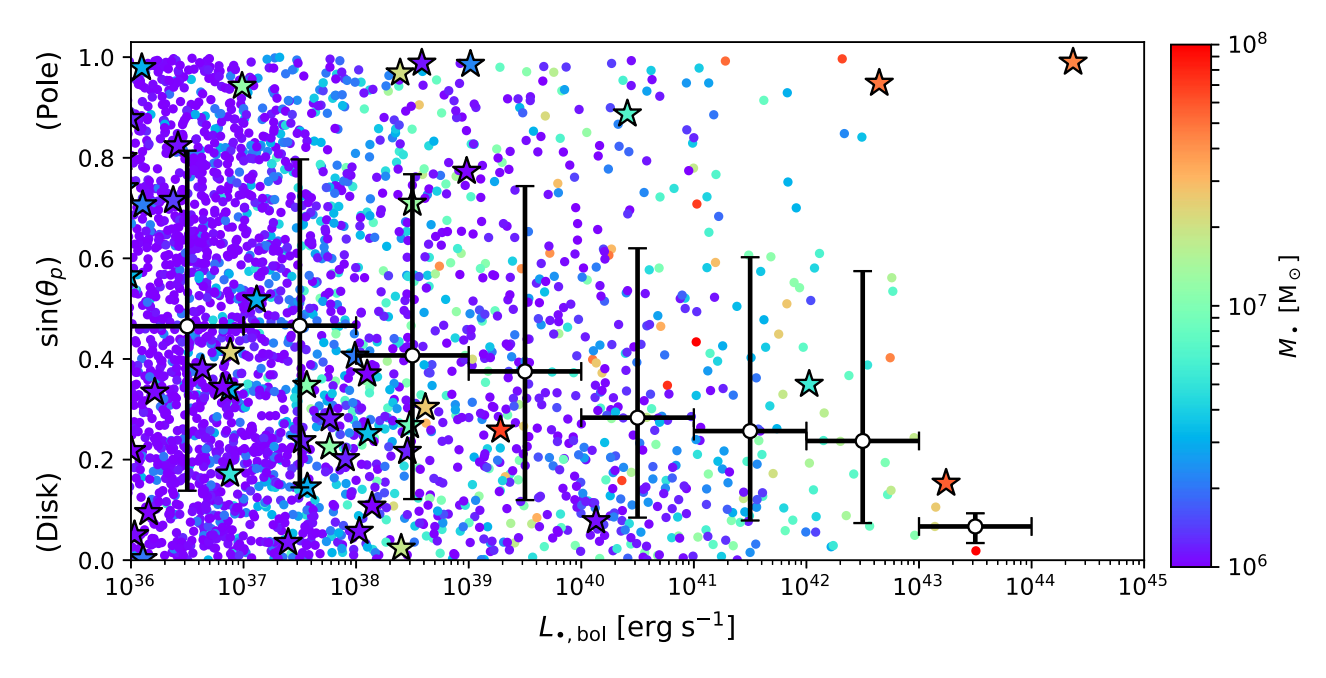


Figure 8. For each wandering SMBH at z = 0.05, we plot $\sin(\theta_p)$ as a function of its bolometric luminosity, where θ_p is the angle made between the SMBH's position vector and the plane of the disk. Points are coloured according to each SMBH's mass. Points marked by stars instead of circles correspond to objects residing in stellar overdensities of a factor of 10 or greater. Error bars span the 16th, 50th, and 84th percentile regions of the objects that do not reside in such overdense regions. This analysis reveals that the more luminous SMBHs are more likely to be more massive and closer to the plane.

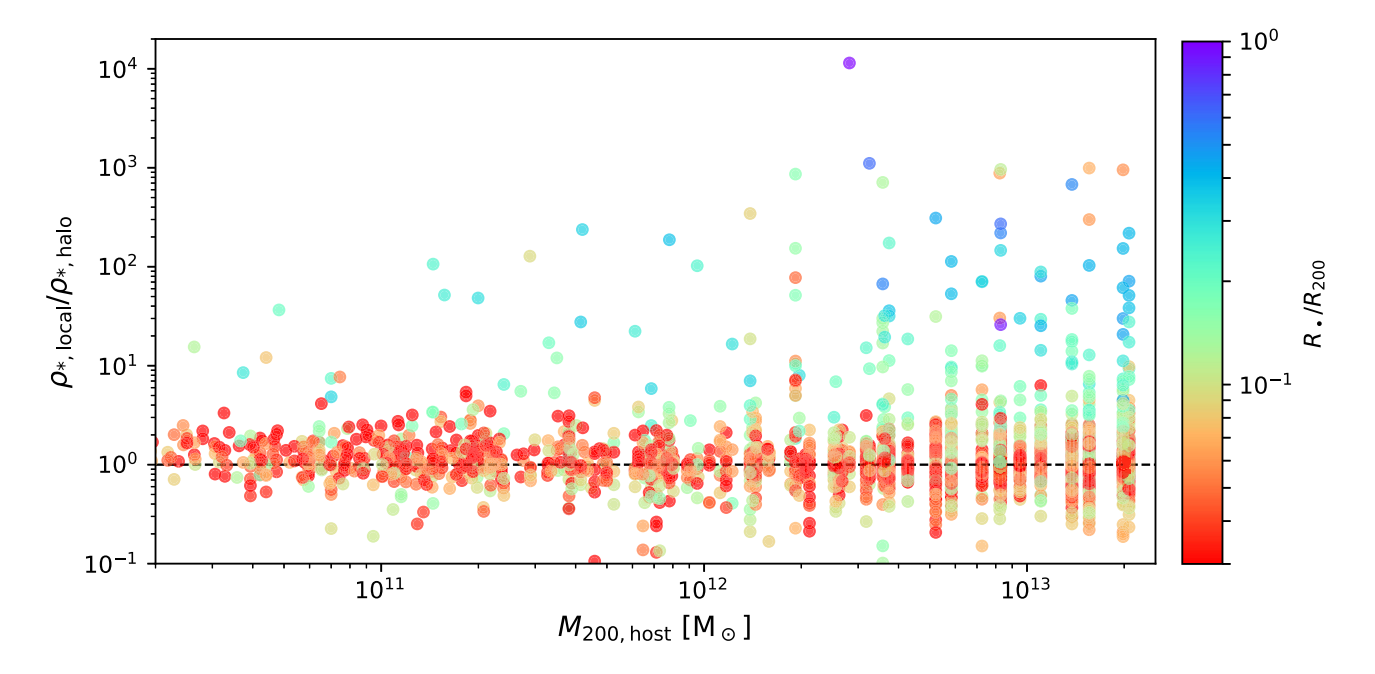


Figure 9. Local stellar overdensity factors of wandering SMBHs as a function of host halo mass at z = 0.05. Colours in this plot encode the ratio of each wanderer's halo-centric distance to the virial radius. Most SMBHs typically do not reside in stellar overdensities in ROMULUS25, except for those at large halo-centric radius. This is consistent with a picture in which wandering SMBHs originate from tidally disrupted satellite haloes.

4.1 The SMBH seeding mechanism

Due to limited resolution, cosmological simulations cannot seed SMBHs at masses lower than those of the other particles in the simulation. The ROMULUS seeding prescription is based on the direct collapse black hole mechanism that may produce 'heavy' seeds up to $\approx\!10^6\,M_{\odot}$ (e.g. Begelman et al. 2006; Lodato & Natarajan 2007),

which is the seed mass employed in these simulations. Alternative 'light' seeding mechanisms also likely operate in the Universe in tandem with or instead of a 'heavy' seeding mechanism (e.g. Madau & Rees 2001; Volonteri et al. 2003). Light seeds, such as the remnants of the first Pop III stars, could be established in greater numbers, but with lower initial masses. Under a light seeding scenario, we

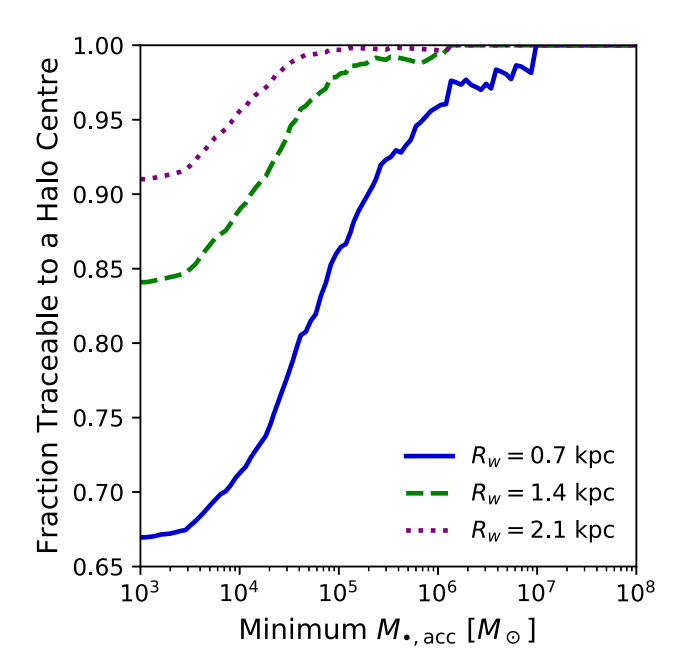


Figure 10. Fraction of wandering SMBHs at z=0.05, above the accreted mass indicated on the *x*-axis, that can be traced back to the centre of any halo. Three values of the halo-centric radius defining the centre of the halo, R_w , are shown. The vast majority of SMBHs can be traced to the centres of haloes at some point earlier in their histories. This demonstrates that ROMULUS does not create spurious seeds, and our wandering SMBHs were once located at the centres of destroyed haloes.

would expect an even greater number of wandering SMBHs, with a mass function extending to lower masses than the $10^6~M_{\odot}$ seeds found in ROMULUS, as explored in detail in (Rashkov & Madau 2014). We reiterate, however, that the heavy seeding mechanism employed by ROMULUS successfully reproduces the observed local SMBH occupation fraction, as shown in Section 3.1.1. Thus, in terms of the census of SMBHs both central and wandering, we believe that the ROMULUS simulations offer a plausible picture, even though we are likely missing SMBHs that originated and grew from light seeds.

Since the ROMULUS seeding prescription is based on local gas properties, one might worry that the wandering SMBHs we find in the simulation may come from spurious seeding sites. To test this, and to gain a better understanding of their origins, we trace back in time the wandering SMBHs at z = 0.05 and examine their host haloes at previous time steps. In Fig. 10, we plot the fraction of SMBHs, above a minimum accreted mass plotted on the x-axis that can be traced to a halo centre at any point in their histories. To be more explicit, for a halo-centric radius R_w beyond which a SMBH is considered wandering, we plot the fraction of wanderers at z = 0.05 that were not wandering at any point in their histories. We confirm that the vast majority of wandering SMBHs originate from the centres of resolved haloes at earlier time slices. This fraction decreases with decreasing accreted mass, meaning that wanderers with greater masses were more likely to have been closer to the centres of a host halo in the past. For the wandering population overall, we report that for R_w of 0.7, 1.4, and 2.1 kpc, the fractions traceable to the halo centre are 67 per cent, 84 per cent, and 91 per cent. In other words, less than 10 per cent of wandering SMBHs have never been within 2.1 kpc of a halo centre. It is even possible for some of wanderers to have been seeded in haloes that formed and were destroyed and/or perturbed by a merger or flyby event in the time between snapshots, causing us to underestimate the fraction traceable to halo centres. Similarly,

it is possible for seeds to form in the centres of overdensities too small and with too few particles to be considered resolved by our strict halo finding criteria. Again, despite the fact that the ROMULUS seeding prescription does not use global halo or galaxy properties, it naturally places SMBHs in halo centres.

4.2 Additional mechanisms to produce wanderers

Due to limited resolution, two additional mechanisms that could potentially produce wanderers are neglected in the Romulus simulations: multibody SMBH interactions (Volonteri et al. 2003; Hoffman & Loeb 2007; Ryu et al. 2018), and gravitational wave recoil from SMBH mergers (Libeskind et al. 2006; Volonteri 2007; Lousto & Zlochower 2011; Blecha et al. 2016). We argue that these additional channels are unlikely to significantly change the average number of wandering SMBHs at a given halo mass. This is because these processes require major galaxy mergers to first form a bound SMBH binary, whereas the wanderers studied in this work originate mainly from prior minor mergers. Since minor mergers always outnumber major ones, the ROMULUS simulations should capture the majority of wandering SMBH population. However, semi-analytic models predict that ejection events can dominate the wandering population at low halo-centric radius (Volonteri & Perna 2005; Izquierdo-Villalba et al. 2020).

4.3 Bondi accretion

Perhaps the greatest uncertainty in the observability of wandering SMBHs is our assumption of Bondi accretion. Recent 3D hydrodynamical simulations suggest that wandering SMBHs fed with hot and diffuse plasma with density fluctuations are limited to 10–20 per cent of the Bondi–Hoyle–Lyttleton accretion rate due to a wide distribution of inflowing angular momentum (Guo et al. 2020). In addition, the accretion rate can be suppressed by several additional orders of magnitude below the Bondi rate due to the accumulation of magnetic flux near the horizon in advection dominated accretion flows (ADAFs; Igumenshchev & Narayan 2002; Perna et al. 2003; Pellegrini 2005; Ressler et al. 2021).

To assess the potential severity of this second effect, we compute the typical Eddington ratios of wandering SMBHs. ADAFs are believed to form around SMBHs accreting at Eddington ratios of $f_{\rm Edd} \lesssim 10^{-3}$, at which point the disk becomes geometrically thick with a lower radiative efficiency (Ichimaru 1977; Rees et al. 1982; Narayan & Yi 1994, 1995; Abramowicz et al. 1995; Reynolds et al. 1996; Yuan & Narayan 2014). The Eddington ratio is given by $f_{\rm Edd} = \dot{M}_{\bullet}/\dot{M}_{\rm Edd}$ for $\dot{M}_{\rm Edd} = 4\pi G M_{\bullet} m_p/\epsilon \sigma_T c$, where G is the gravitational constant, m_p is the proton mass, σ_T is the Thomson cross-section, c is the speed of light, and ϵ is the radiative efficiency. $\dot{M}_{\rm Edd}$ is the mass accretion rate above which radiation pressure inhibits the accumulation of greater mass flux.

We plot the average Eddington ratios as a function of halo mass in Fig. 11 for our different cuts of the wandering population. The top row treats every wandering SMBH equally, whereas the bottom row weights each SMBH according to its accretion rate (averaged over 30 Myr), which is more relevant when considering the emitting population. We find that the typical wandering SMBH exhibits a modest Eddington ratio of $\sim\!10^{-4}$ locally, but that this value increases with increasing redshift, when the universe is denser. However, the emitting population is characterized by much higher Eddington ratios, around 10^{-2} at high redshift. These values may be high enough to avoid the transition to ADAF and suppression of the Bondi rate due to magnetic fields. We also note that the ROMULUS simulations most

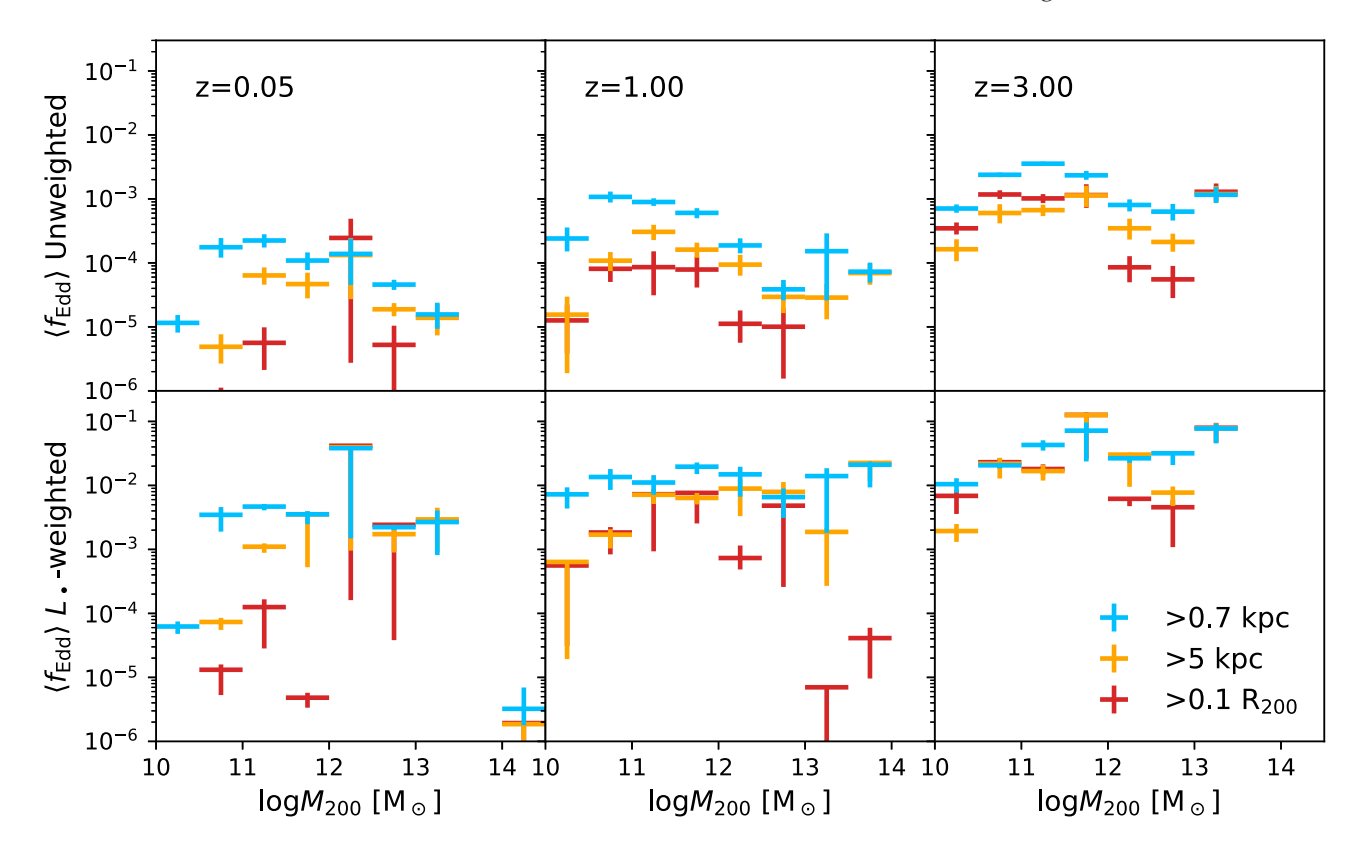


Figure 11. Average Eddington ratios of wandering SMBHs as a function of halo mass for three different redshifts. In the top row, each wandering SMBH is treated equally, while in the bottom row, we weight each wandering SMBH by its accretion rate. The typical wandering SMBH has a modest Eddington ratio of 10^{-4} , but the ones producing detectable emission have Eddington ratios orders of magnitude larger. The typical Eddington ratio increases with redshift, as the universe becomes denser and more gas rich.

likely under-predict the frequency of high Eddington ratio systems, instead producing slow and steady growth proportional to the star formation rate (Ricarte et al. 2019).

5 CONCLUSIONS

We have performed a census of wandering SMBHs in the ROMULUS cosmological simulations. These simulations carefully correct the dynamical friction force on to SMBHs and produces occupation fractions consistent with observations using only local seeding conditions. Our results are summarized below:

- (i) Wandering SMBHs in the ROMULUS simulations originate from the centres of destroyed infalling satellite galaxies. By z=0.05, they do not typically retain a resolvable stellar component in these simulations, but those which do exist at large fractions of their host halo's virial radius.
- (ii) These simulations predict on the order of 10 wandering SMBHs in Milky Way mass haloes at z=0, and their number scales linearly with halo mass, up to 1613 wandering SMBHs in the $10^{14}\,\mathrm{M}_\odot$ main halo of the ROMULUSC cluster simulation.
- (iii) The total mass in wandering SMBHs is roughly 10 per cent the total mass in central SMBHs at z=0.05, but this fraction grows with redshift and even exceeds unity for z>3. Similarly, the total luminosity budget of accreting SMBHs at z>3 is dominated by wanderers. This is likely due to the increased merger rate at high redshift.
- (iv) Wandering SMBHs remain at large radius throughout the dark matter haloes of their hosts. Only roughly half of wandering SMBHs

are within 10 per cent of the virial radius. However, those with larger accretion rates are more likely to be at lower radius, higher mass, and closer to the galactic plane.

(v) Wandering SMBHs in ROMULUS originate from the centres of haloes destroyed in minor mergers. The population is dominated by SMBHs at the seed mass regardless of host halo mass. Most do not retain a resolved stellar counterpart, but those that do tend to be at large fractions of the virial radius, where tidal effects are weaker.

The ROMULUS simulations predict a substantial wandering SMBH population that may even dominate AGN emission at large redshifts. In future work, we will explore the observational signatures of the wandering population in greater detail.

ACKNOWLEDGEMENTS

AR thanks Ramesh Narayan for continued support and insightful conversations about wandering SMBH accretion rates. AR is supported by the National Science Foundation under Grant No. OISE 1743747 as well as the Black Hole Initiative (BHI) by grants from the Gordon and Betty Moore Foundation and the John Templeton Foundation. MT is supported by an NSF Astronomy and Astrophysics Postdoctoral Fellowship under award AST-2001810. PN acknowledges hospitality and support from the Aspen Center for Physics, where some of the early ideas that informed this work were developed during the summer workshop titled "Emergence, Evolution and Effects of Black Holes in the Universe: The Next 50 Years of Black Hole Physics" that she co-organized. The Aspen Center for Physics, is supported by National Science Foundation

grant PHY-1066293. The ROMULUS simulations are part of the Blue Waters sustained-petascale computing project, which is supported by the National Science Foundation (awards OCI-0725070 and ACI-1238993) and the state of Illinois. Blue Waters is a joint effort of the University of Illinois at Urbana-Champaign and its National Center for Supercomputing Applications. This work is also part of a Petascale Computing Resource Allocations allocation support by the National Science Foundation (award number OAC-1613674). This work also used the Extreme Science and Engineering Discovery Environment (XSEDE), which is supported by National Science Foundation grant number ACI-1548562. Resources supporting this work were also provided by the NASA High-End Computing (HEC) Program through the NASA Advanced Supercomputing (NAS) Division at Ames Research Center. Analysis was conducted on the NASA Pleiades computer and facilities supported by the Yale Center for Research Computing.

DATA AVAILABILITY

The data used in the work presented in this article is available upon request to the corresponding author.

REFERENCES

Abramowicz M. A., Chen X., Kato S., Lasota J.-P., Regev O., 1995, ApJ, 438. L37

Afanasiev A. V. et al., 2018, MNRAS, 477, 4856

Ahn C. P. et al., 2017, ApJ, 839, 72

Alexander T., Natarajan P., 2014, Science, 345, 1330

Amaro-Seoane P. et al., 2017, preprint (arXiv:1702.00786)

Ananna T. T., Treister E., Urry C. M., Ricci C., Hickox R. C., Padmanabhan N., Marchesi S., Kirkpatrick A., 2020, ApJ, 889, 17

Armitage P. J., Natarajan P., 2005, ApJ, 634, 921

Arzoumanian Z. et al., 2020, ApJ, 905, L34

Banik U., van den Bosch F. C., Tremmel M., More A., Despali G., More S., Vegetti S., McKean J. P., 2019, MNRAS, 483, 1558

Barausse E., Dvorkin I., Tremmel M., Volonteri M., Bonetti M., 2020, ApJ, 904, 16

Barkana R., Loeb A., 2001, Phys. Rep., 349, 125

Barrows R. S., Mezcua M., Comerford J. M., 2019, ApJ, 882, 181

Bartlett D. J., Desmond H., Devriendt J., Ferreira P. G., Slyz A., 2021, MNRAS, 500, 4639

Begelman M. C., Blandford R. D., Rees M. J., 1980, Nature, 287, 307

Begelman M. C., Volonteri M., Rees M. J., 2006, MNRAS, 370, 289

Bellovary J. M., Governato F., Quinn T. R., Wadsley J., Shen S., Volonteri M., 2010, ApJ, 721, L148

Bellovary J., Volonteri M., Governato F., Shen S., Quinn T., Wadsley J., 2011, ApJ, 742, 13

Bellovary J. M. et al., 2021, preprint (arXiv:2102.09566)

Biernacki P., Teyssier R., Bleuler A., 2017, MNRAS, 469, 295

Blecha L. et al., 2016, MNRAS, 456, 961

Bocquet S., Saro A., Dolag K., Mohr J. J., 2016, MNRAS, 456, 2361

Bondi H., 1952, MNRAS, 112, 195

Booth C. M., Schaye J., 2009, MNRAS, 398, 53

Bortolas E., Capelo P. R., Zana T., Mayer L., Bonetti M., Dotti M., Davies M. B., Madau P., 2020, MNRAS, 498, 3601

Bromm V., Loeb A., 2003, ApJ, 596, 34

Callegari S., Mayer L., Kazantzidis S., Colpi M., Governato F., Quinn T., Wadsley J., 2009, ApJ, 696, L89

Callegari S., Kazantzidis S., Mayer L., Colpi M., Bellovary J. M., Quinn T., Wadsley J., 2011, ApJ, 729, 85

Chandrasekhar S., 1943, ApJ, 97, 255

Colpi M., 2014, Space Sci. Rev., 183, 189

Comerford J. M. et al., 2009, ApJ, 698, 956

Comerford J. M., Schluns K., Greene J. E., Cool R. J., 2013, ApJ, 777, 64

Croton D. J. et al., 2006, MNRAS, 365, 11

Davé R., Anglés-Alcázar D., Narayanan D., Li Q., Rafieferantsoa M. H., Appleby S., 2019, MNRAS, 486, 2827

Dayal P., Rossi E. M., Shiralilou B., Piana O., Choudhury T. R., Volonteri M., 2019, MNRAS, 486, 2336

Devecchi B., Volonteri M., 2009, ApJ, 694, 302

Di CintioA., Tremmel M., Governato F., Pontzen A., Zavala J., Bastidas Fry A., Brooks A., Vogelsberger M., 2017, MNRAS, 469, 2845

Di Matteo T., Springel V., Hernquist L., 2005, Nature, 433, 604

Dosopoulou F., Antonini F., 2017, ApJ, 840, 31

Dubois Y. et al., 2014, MNRAS, 444, 1453

Dubois Y., Peirani S., Pichon C., Devriendt J., Gavazzi R., Welker C., Volonteri M., 2016, MNRAS, 463, 3948

Dvorkin I., Barausse E., 2017, MNRAS, 470, 4547

Escala A., Larson R. B., Coppi P. S., Mardones D., 2004, ApJ, 607, 765

Ferrarese L., Merritt D., 2000, ApJ, 539, L9

Fiacconi D., Mayer L., Roškar R., Colpi M., 2013, ApJ, 777, L14

Fujita Y., 2008, ApJ, 685, L59

Fujita Y., 2009, ApJ, 691, 1050

Gebhardt K. et al., 2000, ApJ, 539, L13

Goicovic F. G., Sesana A., Cuadra J., Stasyszyn F., 2017, MNRAS, 472, 514

Governato F., Colpi M., Maraschi L., 1994, MNRAS, 271, 317

Gualandris A., Read J. I., Dehnen W., Bortolas E., 2017, MNRAS, 464, 2301

Guo M., Inayoshi K., Michiyama T., Ho L. C., 2020, ApJ, 901, 39

Haehnelt M. G., Natarajan P., Rees M. J., 1998, MNRAS, 300, 817

Hobbs G. et al., 2010, Class. Quantum Gravity, 27, 084013

Hoffman L., Loeb A., 2007, MNRAS, 377, 957

Hopkins P. F., Richards G. T., Hernquist L., 2007, ApJ, 654, 731

Ichimaru S., 1977, ApJ, 214, 840

Igumenshchev I. V., Narayan R., 2002, ApJ, 566, 137

Izquierdo-Villalba D., Bonoli S., Dotti M., Sesana A., Rosas-Guevara Y., Spinoso D., 2020, MNRAS, 495, 4681

Joshi G. D., Parker L. C., Wadsley J., 2016, MNRAS, 462, 761

Kauffmann G., Haehnelt M., 2000, MNRAS, 311, 576

Kawaguchi T., Saito Y., Miki Y., Mori M., 2014, ApJ, 789, L13

Khan F. M., Holley-Bockelmann K., Berczik P., Just A., 2013, ApJ, 773, 100

King A. R., Dehnen W., 2005, MNRAS, 357, 275

Klein A. et al., 2016, Phys. Rev. D, 93, 024003

Knollmann S. R., Knebe A., 2009, ApJS, 182, 608 Kormendy J., Ho L. C., 2013, ARA&A, 51, 511

Kormendy J., Richstone D., 1995, ARA&A, 33, 581

Kulier A., Ostriker J. P., Natarajan P., Lackner C. N., Cen R., 2015, ApJ, 799, 178

Libeskind N. I., Cole S., Frenk C. S., Helly J. C., 2006, MNRAS, 368, 1381

Lodato G., Natarajan P., 2006, MNRAS, 371, 1813

Lodato G., Natarajan P., 2007, MNRAS, 377, L64

Lousto C. O., Zlochower Y., 2011, Phys. Rev. D, 83, 024003

Ma L., Hopkins P. F., Ma X., Anglés-Alcázar D., Faucher-Giguère C.-A., Kelley L. Z., 2021, preprint (arXiv:2101.02727)

Madau P., Rees M. J., 2001, ApJ, 551, L27

Mayer L., Kazantzidis S., Madau P., Colpi M., Quinn T., Wadsley J., 2007, Science, 316, 1874

Menon H., Wesolowski L., Zheng G., Jetley P., Kale L., Quinn T., Governato F., 2015, Comput. Astrophys. Cosmol., 2, 1

Merloni A., Heinz S., 2008, MNRAS, 388, 1011

Mezcua M., Domínguez Sánchez H., 2020, ApJ, 898, L30

Micic M, Holley-Bockelmann K, Sigurdsson S, 2011, MNRAS, 414, 1127 Miller B. P., Gallo E., Greene J. E., Kelly B. C., Treu T., Woo J.-H., Baldassare

Ailler B. P., Gallo E., Greene J. E., Kelly B. C., Treu T., Woo J.-H., Baldassa V., 2015, ApJ, 799, 98

Milosavljević M., Merritt D., 2001, ApJ, 563, 34

Milosavljević M., Merritt D., 2003, in Centrella J. M., ed., AIP Conf. Proc. Vol. 686, The Astrophysics of Gravitational Wave Sources. Am. Inst. Phys., New York, p. 201

Moster B. P., Naab T., White S. D. M., 2013, MNRAS, 428, 3121

Narayan R., Yi I., 1994, ApJ, 428, L13

Narayan R., Yi I., 1995, ApJ, 452, 710

Natarajan P., 2014, Gen. Relativ. Gravit., 46, 1702

Natarajan P., 2021, MNRAS, 501, 1413

Neumayer N., Seth A., Böker T., 2020, A&AR, 28, 4

Oh S. P., Haiman Z., 2002, ApJ, 569, 558

Ostriker E. C., 1999, ApJ, 513, 252

Pacucci F., Loeb A., 2020, ApJ, 895, 95

Pellegrini S., 2005, ApJ, 624, 155

Perna R., Narayan R., Rybicki G., Stella L., Treves A., 2003, ApJ, 594, 936

Pfister H., Volonteri M., Dubois Y., Dotti M., Colpi M., 2019, MNRAS, 486, 101

Pillepich A. et al., 2018, MNRAS, 473, 4077

Pontzen A., Tremmel M., 2018, ApJS, 237, 23

Pontzen A., Roškar R., Stinson G. S., Woods R., Reed D. M., Coles J., Quinn T. R., 2013, pynbody: N-Body/SPH analysis for python, Astrophysics Source Code Library, record ascl:1305.002

Power C., Navarro J. F., Jenkins A., Frenk C. S., White S. D. M., Springel V., Stadel J., Quinn T., 2003, MNRAS, 338, 14

Rantala A., Pihajoki P., Johansson P. H., Naab T., Lahén N., Sawala T., 2017, ApJ, 840, 53

Rashkov V., Madau P., 2014, ApJ, 780, 187

Rees M. J., Begelman M. C., Blandford R. D., Phinney E. S., 1982, Nature, 295, 17

Reines A. E., Volonteri M., 2015, ApJ, 813, 82

Reines A. E., Condon J. J., Darling J., Greene J. E., 2020, ApJ, 888, 36

Ressler S. M., Quataert E., White C. J., Blaes O., 2021, MNRAS, preprint (arXiv:2102.01694)

Reynolds C. S., Di Matteo T., Fabian A. C., Hwang U., Canizares C. R., 1996, MNRAS, 283, L111

Ricarte A., Natarajan P., 2018a, MNRAS, 474, 1995

Ricarte A., Natarajan P., 2018b, MNRAS, 481, 3278

Ricarte A., Tremmel M., Natarajan P., Quinn T., 2019, MNRAS, 489, 802

Ryu T., Perna R., Haiman Z., Ostriker J. P., Stone N. C., 2018, MNRAS, 473, 3410

Saglia R. P. et al., 2016, ApJ, 818, 47

Schaye J. et al., 2015, MNRAS, 446, 521

Schneider R., Ferrara A., Natarajan P., Omukai K., 2002, ApJ, 571, 30

Schramm M., Silverman J. D., 2013, ApJ, 767, 13

Sesana A., Volonteri M., Haardt F., 2007, MNRAS, 377, 1711

Seth A. C. et al., 2014, Nature, 513, 398

Shankar F. et al., 2016, MNRAS, 460, 3119

Shen X., Hopkins P. F., Faucher-Giguère C.-A., Alexander D. M., Richards G. T., Ross N. P., Hickox R. C., 2020, MNRAS, 495, 3252

Sijacki D., Springel V., Di Matteo T., Hernquist L., 2007, MNRAS, 380, 877

Sijacki D., Springel V., Haehnelt M. G., 2011, MNRAS, 414, 3656

Soltan A., 1982, MNRAS, 200, 115

Somerville R. S., Hopkins P. F., Cox T. J., Robertson B. E., Hernquist L., 2008, MNRAS, 391, 481

Springel V., Di Matteo T., Hernquist L., 2005, MNRAS, 361, 776

Steinborn L. K., Dolag K., Comerford J. M., Hirschmann M., Remus R.-S., Teklu A. F., 2016, MNRAS, 458, 1013

Tamfal T., Capelo P. R., Kazantzidis S., Mayer L., Potter D., Stadel J., Widrow L. M., 2018, ApJ, 864, L19

Tremaine S. et al., 2002, ApJ, 574, 740

Tremmel M., Governato F., Volonteri M., Quinn T. R., 2015, MNRAS, 451, 1868

Tremmel M., Karcher M., Governato F., Volonteri M., Quinn T. R., Pontzen A., Anderson L., Bellovary J., 2017, MNRAS, 470, 1121

Tremmel M., Governato F., Volonteri M., Quinn T. R., Pontzen A., 2018a, MNRAS, 475, 4967

Tremmel M., Governato F., Volonteri M., Pontzen A., Quinn T. R., 2018b, ApJ, 857, L22

Tremmel M. et al., 2019, MNRAS, 483, 3336

van den Bosch F. C., Ogiya G., 2018, MNRAS, 475, 4066

Van Wassenhove S., Capelo P. R., Volonteri M., Dotti M., Bellovary J. M., Mayer L., Governato F., 2014, MNRAS, 439, 474

Voggel K. T., Seth A. C., Baumgardt H., Mieske S., Pfeffer J., Rasskazov A., 2019, ApJ, 871, 159

Volonteri M., 2007, ApJ, 663, L5

Volonteri M., Perna R., 2005, MNRAS, 358, 913

Volonteri M., Haardt F., Madau P., 2003, ApJ, 582, 559

Volonteri M., Madau P., Quataert E., Rees M. J., 2005, ApJ, 620, 69

Volonteri M., Sikora M., Lasota J. P., Merloni A., 2013, ApJ, 775, 94

Wadsley J. W., Keller B. W., Quinn T. R., 2017, MNRAS, 471, 2357

Wang X., Loeb A., 2014, MNRAS, 441, 809

Yuan F., Narayan R., 2014, ARA&A, 52, 529

Zivancev C., Ostriker J., Küpper A. H. W., 2020, MNRAS, 498, 3807

This paper has been typeset from a $T_EX/I = T_EX$ file prepared by the author.